SAND2017-10681C

Determining the internal pressure in 18650 format lithium batteries under thermal abuse

Frank Austin Mier[1], Dr. Michael Hargather[1], and Dr. Summer Ferreira[2]

[1]*New Mexico Tech, Socorro, NM*
[2]*Sandia National Laboratories, Albuquerque, NM*

September 7, 2017

Abstract

Lithium batteries have a well-known tendency to fail violently under abuse conditions which can result in venting of flammable material. Understanding these events can aid in evaluating safety associated with individual battery cells and battery packs when these fluids are vented. The external fluid dynamics of the venting process, including liquid droplets and gases, is directly related to the internal pressure of the battery cell. In this work, battery case strain is measured on cells under thermal abuse which is then used to calculate the internal pressure via hoop and longitudinal stress relations. Strain measurement is a non-invasive approach which will have no bearing on the decomposition within batteries that leads to thermal runaway. Complementary tests are performed to confirm the strain-pressure relationship by pressurizing 18650 cell caps to failure with an inert fluid. A laboratory setup with a heated test chamber was designed and fabricated to remotely subject cells to heating rates up to 6 °C/min. Additional measurements include cell temperature and the test chamber pressure, temperature, and heat flux. Variables explored in these tests include cell chemistry, state of charge, and heating rate.

Keywords— Internal pressure, Abuse testing, Cell venting, Lithium battery, Safety

1 Introduction

Internal pressure within a battery is an important parameter in describing if and how the venting process will occur when a battery has been subjected to thermal abuse. Among other parameters including opening area and density, pressure is key in describing the venting liquid and gas flow fields as well as the criteria for the onset of atomization of vented liquids [1, 2]. Prior work has documented the processes within lithium batteries which occur under thermal abuse with various calorimetry and chemical analysis methods [3]. These tests have also produced experimental measurements on the pressure increase within an enclosed space associated with the venting of 18650 cells. Additional research has performed X-ray computed tomographic imaging within 18650 format cells during thermal runaway to show the gas generation process taking place [4]. A generic burst pressure value of 3,448 kPa has been represented in modeling venting of 18650 cells which includes the use of a choked flow condition at the vent [5]. However, it is important to understand the pressures at which different cell types open, the consistency of the opening pressure, and how the pressure builds up within the cell throughout failure process.

Current research presented here includes two complementary experiments to measure the internal pressure characteristics of 18650 format lithium batteries under thermal abuse conditions. A direct pressurization experiment has been designed to measure the burst pressure and opening area of the vent cap located at the positive terminal of the cells. Another test setup has been constructed to measure the case strain of a battery throughout an entire thermal abuse test to measure the in internal pressure time history. From analytical expressions, the non-invasive strain measurements can be used to infer the internal pressure of within the battery at any moment.

2 Direct pressurization test methodology

2.1 Test apparatus design and instrumentation

Typical battery construction includes a vent mechanism that is crimped in place as part of the positive terminal of a cell. The vents tested here are removed from actual cells using a pipe cutter to separate the cap from the outer battery case. The foil tab which electrically connects the vent cap to the cathode material is then cut, thus completely separating the battery cap. This method is chosen as the entire vent mechanism is left intact. Once removed from the cells, the vent caps retain the battery diameter of 18 mm and have an axial thickness of approximately 4.5 mm. Figure 2.1 shows an image of the cap in place on the cell and then removed for direct pressurization testing.

The test apparatus designed and tested here is intended to securely hold vent caps once removed from a battery and create an airtight seal with a source of pressurized air, as shown in Figure 2.2. A single vent cap is held firmly between two 7/8-14 UNF sized set screws, and gaskets are used to create a seal. The set screws have a 12.7 mm interior hexagon which allows for fastening while leaving a central opening for unobstructed air flow out of the vents. This design allows for the battery cap to vary in height due differences in manufacturing tolerance and removal procedure. The cap holder can also accept caps up to 20.6 mm in

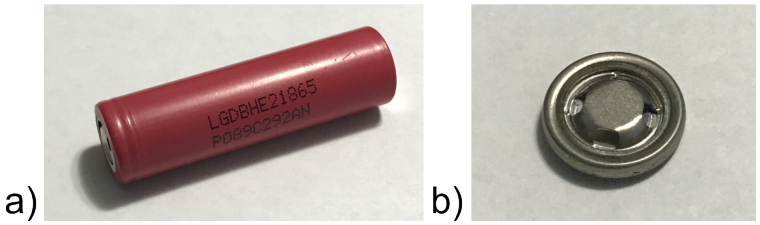

Figure 2.1: (a) An intact 18650 format battery (LG HE2) and (b) the vent cap after removal.

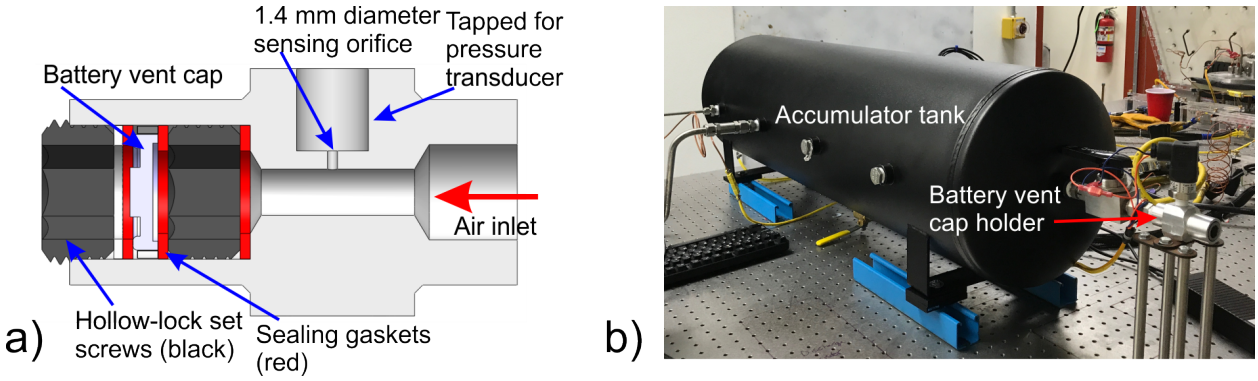

Figure 2.2: (a) Schematic representation of the battery vent cap holder and (b) the completed test setup installed at New Mexico Tech.

diameter. A short length of tubing connects the battery cap fixture to a tank which is connected to a pressure regulated source of dry air.

The center of the battery holder is machined to a precisely known cross-sectional area. A small sensing orifice with a diameter of 1.4 mm allows for measurement of static pressure throughout testing. This feature provides the ability to calculate the opening area of each vent cap. The cross sectional area at the sensing orifice of 40.0 mm^2 is chosen to be larger than the maximum possible opening area of a battery vent cap, based on a survey of battery end cap designs for cells of interest. This ensures that when venting flow will choke at the vent cap rather than anywhere else within the system.

The direct pressurization test setup is shown in Figure 2.2(b). Major components included in this setup are the previously described battery vent cap holder, an accumulator tank, pressure regulator, and compressed air cylinder. Air from the cylinder is used to pressurize the tank, vent cap holder, and thus the battery cap itself to a regulated level. While the vent cap has not yet opened, the air within the tank and vent cap holder has no significant velocity as the regulated pressure level is able to be increased very slowly. The accumulator tank has a volume of 76 L which is chosen to minimize transience in pressure values once the vent has opened. A pressure transducer and exposed junction, K-type thermocouple are placed at the opposite end of the accumulator tank from the vent cap holder to measure stagnation pressure and temperature respectively. This location is chosen as gas velocities will be approximately zero at this location once the vent cap opens. Additionally, before vent opening both pressure transducers will be measuring a stagnation pressure as no flow has occurred yet. Once the battery vent opens, the static and stagnation pressure

data readings will diverge. Temperature and pressure data are recorded and monitored simultaneously with a National Instruments cDAQ data acquisition system and LabVIEW. Data acquisition rates for the temperature and pressure measurements are 100 Hz and 1 kHz respectively.

2.2 Calculation of opening area

The opening area of the vent cap is inferred via the measured relationship between static and stagnation pressures. Within the test setup, three distinct locations are considered in the analysis: stagnation within the tank, the known cross-section in the vent cap holder, and the opening in the battery vent itself. In most tests, it is expected that the pressure required for the vent to open is also enough to create a choked flow condition. For this to occur, the absolute pressure to open the vent must be 1.89 times atmospheric pressure or greater [6]. As this pressure differential creates a choked flow, it is known that the Mach number of air passing through the vent cap will be fixed at unity until the stagnation pressure drops below 76 kPa gauge (using a value of 86 kPa for atmospheric pressure as measured in the laboratory). The flow will choke at the battery vent cap because it was intentionally designed to have the smallest cross-sectional area within the system.

Once the vent opens and allows air to leave the system, the static pressure measurement taken in the vent cap holder (P_1) will be lower than the stagnation pressure (P_0) at any given instant. Making the assumptions that the flow within the system is isentropic and the air behaves as an ideal gas, the Mach (M_1) number of the flow through the vent cap holder can be calculated via the isentropic flow relation in Equation 2.1 where γ is the ratio of specific heats [6, 7]:

$$\frac{P_0}{P_1} = \left(1 + \frac{\gamma + 1}{2} M_1^2\right)^{\frac{\gamma}{\gamma - 1}} \tag{2.1}$$

Once the calculation of Mach number through the vent cap holder is complete, it can be used along with the known cross-sectional area at this location (A_1) and Equation 2.2 to calculate the area at which the flow is choked (A^*), which is the vent area:

$$\frac{A_1}{A^*} = \frac{1}{M_1} \left(\frac{\frac{\gamma+1}{2}}{1 + \frac{\gamma-1}{2} M_1^2}\right)^{\frac{\gamma+1}{2-2\gamma}} \tag{2.2}$$

If the flow is no longer choked at the vent opening, the Equations 2.1 and 2.2 can still be used with the additional assumption that the flow exits the system through the vent cap with static pressure equal to atmospheric pressure. Accordingly, Mach numbers can be calculated at the vent cap holder (M_1) and vent cap (M_2). Equation 2.2 will provide area ratios A_2/A^* and A_1/A^* at these two locations. Letting A^* become an arbitrary location for the sonic condition, the vent cap opening area (A_2) can be calculated in terms of the known value for A_1.

2.3 Validation series with known orifices

A series of orifice plates were fabricated for validation of the opening area calculation methodology. These plates were installed and tested as direct substitutes for the battery vent cap in the test setup. Twenty circular orifices ranging in area from 3.16 mm^2 to 37.4 mm^2 were tested. Additionally, three mock vent orifices seen in Figure 2.3 were created representing the intricate geometry and maximum opening area of cells from LG, Panasonic, and A123. The maximum opening area was taken as the series of cutouts on the innermost portion of the vent cap.

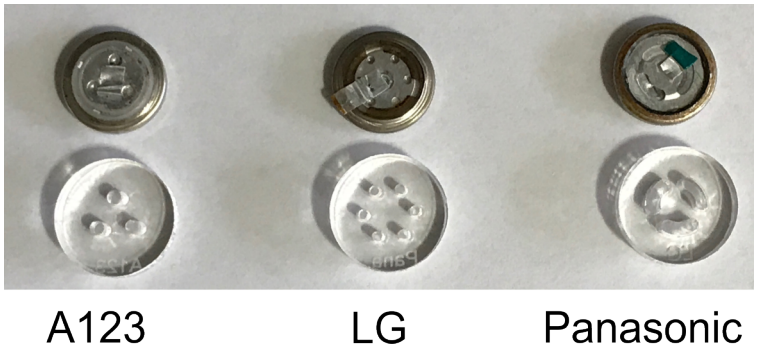

Figure 2.3: The internal surface of battery vent caps from 18650 format cells made by LG, Panasonic, and A123 and orifice plates made to mimic the maximum possible opening area.

While tests with battery caps will start from zero gauge pressure within the sealed system and increased until vent opening, the orifice plates do not have a venting mechanism. As such, a ball valve installed between the accumulator tank and the orifice plate was used to manually simulate the opening of a battery vent. To eliminate any erroneous pressure data due to opening the ball valve, the first two seconds stagnation and static pressure readings are ignored. All tests begin with the accumulator tank at approximately 276 kPa to provide a significant amount of time in which the flow is choked.

Initially, three of the twenty circular orifices were chosen for repeated trials to confirm the consistency of the system. The three orifices have areas of 18.5 mm^2, 27.7 mm^2, and 34.5 mm^2 which correspond to standard drill sizes of 11, A, and G respectively. Each orifice was tested five times, and the measured ratio between static and stagnation pressures was used to calculate the opening area. The results of these tests shown in Table 2.1 demonstrate the accuracy and repeatability of this experiment.

Individual trials performed on each of the circular orifices show strong agreement between actual and experimentally calculated opening areas throughout the range of possible vent cap opening areas. The results of this validation series are presented in Figure 2.4. The orifices designed to resemble the battery vent caps in Figure 2.3 show similarly accurate agreement between the actual and calculated opening area.

Table 2.1: Opening area results from repeated trials

Test	Actual area (mm^2)	Calculated area (mm^2)	Error (%)
11 Drill, Run 1	18.5	19.4	5.1
11 Drill, Run 2	18.5	19.5	5.3
11 Drill, Run 3	18.5	19.5	5.3
11 Drill, Run 4	18.5	19.6	5.9
11 Drill, Run 5	18.5	19.7	6.3
A Drill, Run 1	27.7	28.2	1.6
A Drill, Run 2	27.7	28.3	1.9
A Drill, Run 3	27.7	28.3	1.9
A Drill, Run 4	27.7	28.4	2.2
A Drill, Run 5	27.7	28.4	2.2
G Drill, Run 1	34.5	34.4	0.4
G Drill, Run 2	34.5	34.4	0.4
G Drill, Run 3	34.5	34.4	0.4
G Drill, Run 4	34.5	34.4	0.4
G Drill, Run 5	34.5	34.4	0.4

3 Design and construction of a strain measurement test fixture

3.1 Theoretical basis of experiment

Strain gauges are used here to perform noninvasive measurement of batteries under thermal abuse conditions. These gauges are adhered to the battery case with a high temperature rated cyanoacrylate glue as seen in Figure 3.1. Fundamentally, a strain gauge operates by changing electrical resistance when it is deformed, which is easily measured by a commercial data acquisition system. Strain measurement allows data to be recorded throughout the entire abuse and eventual thermal runaway process without a need to modify cells which could inherently change how they may react to abuse. The generic nature of this testing approach allows for experiments to be performed on cells of different chemistries and manufacturers.

By treating the outer casing of the battery as a thin walled cylinder, analytic expressions relate hoop (σ_H) and longitudinal (σ_L) stress to the internal pressure (P) within the cell as described by Equations 3.1 and 3.2 [8]:

$$\sigma_H = \frac{PD}{2t} \tag{3.1}$$

$$\sigma_L = \frac{PD}{4t} \tag{3.2}$$

These equations contain easily measurable geometric constants for the cylindrical battery diameter (D) and case thickness (t). These two stress parameters are converted to strain

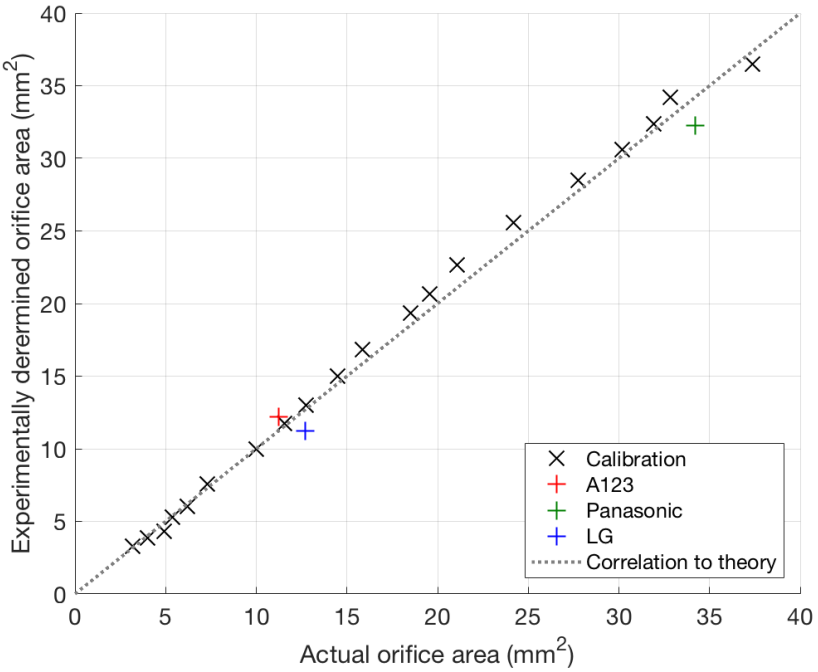

Figure 2.4: Comparison between actual and calculated opening areas from the validation series performed on the direct pressurization test apparatus. Both circular and more complex geometries of actual vent can be measured accurately with this methodology.

via the Young's Modulus for the given case material (E). By measuring strain of a battery case under abuse conditions, the internal pressure is inferred.

An important experimental consideration within the range of temperatures observed in thermal runaway events is thermal expansion. The strain measured in experiments can be taken as the sum of the components due to changes in internal pressure and temperature [9]. Expansion along the length and circumference increases the longitudinal and hoop strain measurements respectively. Changes to the length (dl) and circumference (dc) to the battery case as a result of a finite temperature increase (dT) are both forms of linear thermal expansion as described in Equations 3.3 and 3.4 [10]:

$$dc = \alpha \pi D_0 dT \tag{3.3}$$

$$dl = \alpha l_0 dT \tag{3.4}$$

The subscript 0 denotes the initial battery length and diameter. The coefficient of thermal expansion (α) is a material property and assumed constant over the temperature changes expected.

By noting that engineering strain (ϵ) is defined as the change in length to the original length of an object, Equations 3.3 and 3.4 may be rearranged to show that the component of case strain due to changes in temperature may be expressed as the product of the thermal expansion coefficient and the finite temperature change. Summing the components of strain

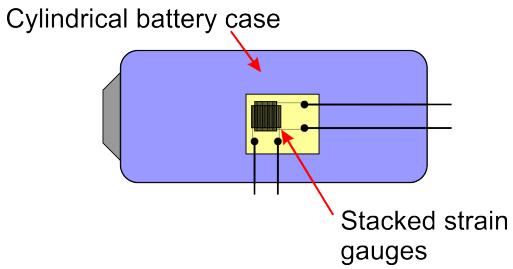

Figure 3.1: A schematic representation of the arrangement for how two stacked strain gauges can be mounted to a cylindrical battery. The gauge orientation shown would be used to measure hoop and longitudinal strain.

due to internal pressure and temperature increases gives Equations 3.5 and 3.6:

$$\epsilon_H = E\frac{PD}{2t} + \alpha dT \tag{3.5}$$

$$\epsilon_L = E\frac{PD}{4t} + \alpha dT \tag{3.6}$$

Equations 3.5 and 3.6 represent the measurements that would be taken by strain gauges mounted to a battery as it undergoes thermal abuse. Rearranging these two relations provides Equation 3.7.

$$P = \frac{t}{4ED}\left(\epsilon_H - \epsilon_L\right) \tag{3.7}$$

This expression states that the internal pressure is proportional to the difference of the two strain measurements. Values for cell diameter, case thickness, or Young's Modulus can be measured directly but may require cell disassembly and material testing. However, these parameters may be estimated if experimental strain data can be fixed to a known pressure state of the cell. This could be the battery state at the moment of venting onset where strain is expected to reach a maximum value which can be related to the directly measured burst pressure described in Section 2. Variability in this estimation between pressure and strain states would be influenced by the results of the direct pressurization testing.

Limitations of this approach could include localized failures within the cell. This could include deformations of interior battery components associated with events such as an internal short. Additionally, as gas generation can be localized within the cell prior to failure (e.g. trapped between anode and cathode layers), leading to nonuniform pressure distribution. To address this, initial tests will be performed with multiple sets of strain gauges on a single cell.

3.2 Design of laboratory test setup

A test facility was designed and constructed to measure the external case strain of 18650 format batteries under thermal abuse conditions. The test setup consists of a heated cylindrical chamber with ports for instrumentation and a viewing window seen in Figure 3.2(a). A 4 NPT size Schedule 160 steel pipe section is used to create the body of the chamber,

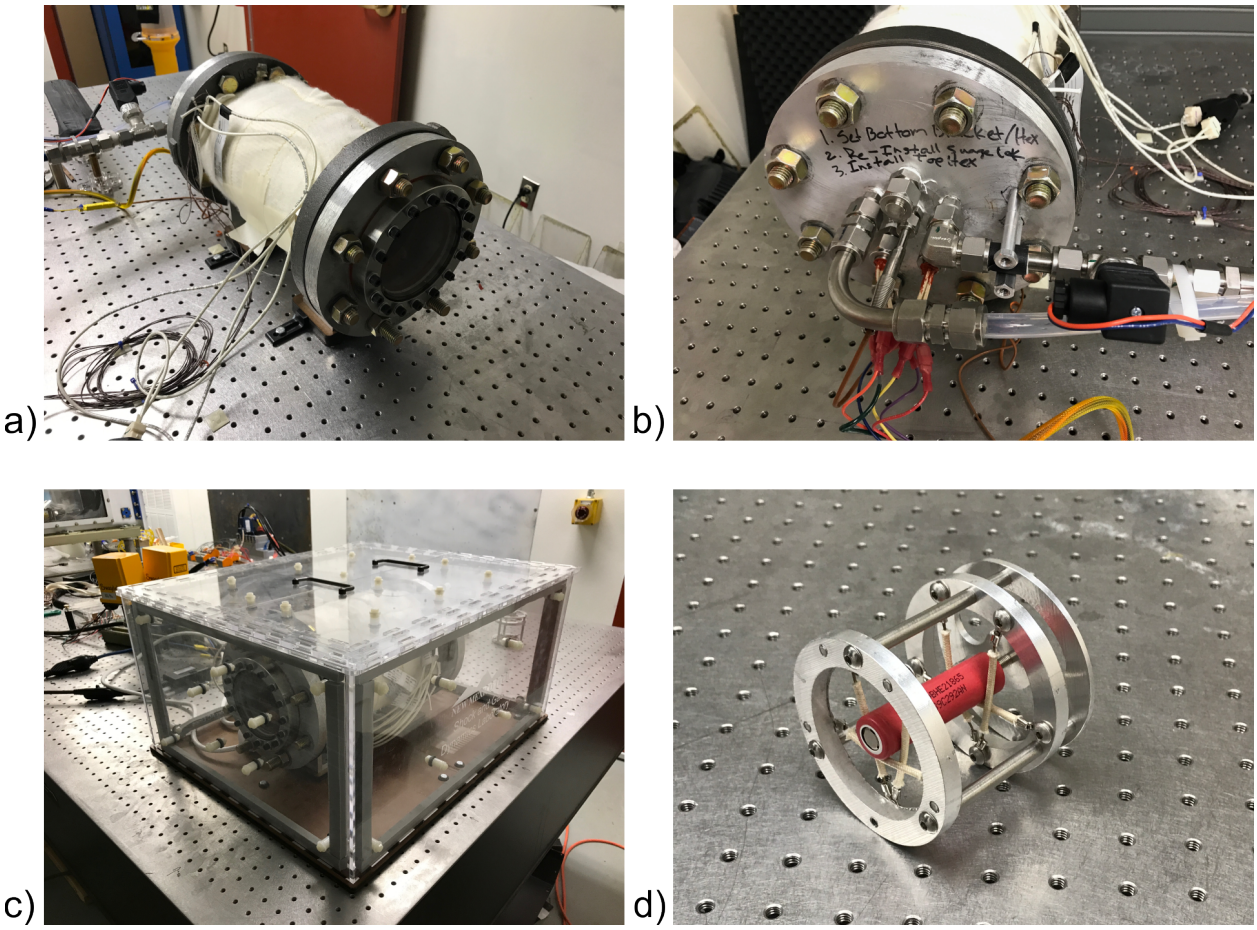

Figure 3.2: Images of the test setup installed at New Mexico Tech including (a) the test chamber, (b) instrumentation end cap, (c) insulation structure, and (d) battery holder.

and standard pipe flanges are threaded to the ends to provide rigid mounting points for removable end caps. The interior space within the chamber is 87 mm in diameter by 305 mm long. There are dedicated end caps for viewing the battery throughout testing and allowing instrumentation pass-throughs. Figure 3.2(b) shows the completed instrumentation end cap which has ports for a thermocouple probe to measure chamber gas temperature, three reconfigurable passthroughs for thermocouples and and strain gauge leads, and an inlet and outlet for a remote purge system. Additionally, thermocouples are embedded into the main body of the test chamber to measure the temperature gradient within the steel and thus allow calculation of heat flux.

Preliminary testing of the chamber highlighted a need for high total power output from chamber heaters and sufficient insulation of the test chamber. The chamber body is evenly wrapped with nine electrical rope heaters each capable of outputting 260 W as to create even heating within the chamber interior. As achieving relatively high heating rates is important within the chamber to be able to subject batteries to different abuse scenarios, work has gone into insulating the test chamber. A flexible insulation wrap made of fiberglass, ceramic fiber, and Nomex is placed around the test chamber body immediately outside of the rope heaters and secured with stainless steel pipe clamps. The test chamber itself is also placed

inside of another rigid insulation structure seen in Figure 3.2(c). This structure is fabricated from laser cut acrylic sheeting and has a modular design of double-pane panels. A final step taken in improving heat transfer to batteries is the use of a helium environment inside the chamber. This improves heat transfer significantly as helium has a relatively high thermal conductivity value of 0.142 W/mK compared to a value of 0.024 W/mK for air.

A battery holder was designed and fabricated to securely hold a cell prior to and during venting within the center of the test chamber. Seen in Figure 3.2(d), the holder uses high temperature MG wire with a series of aluminum rings and standoffs. This holder fits within inner diameter of the test chamber with minimal movement. The cradle shape of the wire is designed to allow the battery to expand freely throughout testing as to not cause any stress concentrations which would negatively affect strain measurements. A thumb nut and set screw are used in the last aluminum ring to create a hard stop for the battery in case venting causes a thrust which would otherwise cause the cell to move inside the chamber.

Data acquisition is performed with a National Instrument cDAQ system and controlled through LabVIEW. The system is configured to record temperature, strain, and pressure data as well as control the operation of inlet and exit valves used for remote purge of the gas within the chamber after a test. Four J-type thermocouples are embedded in pairs on opposite sides of the chamber wall. Each pair has a thermocouple at a depth of 3.3 mm and 10.1 mm which correspond to roughly 25% and 75% of the wall thickness respectively. K-type thermocouples are used to measure interior chamber gas temperature and surface temperature of the battery on the side of the case and on the positive terminal at the end of the vent cap. Chamber static pressure is also recorded and monitored throughout testing Each strain gauge is wired in a three-wire, quarter bridge configuration with 350 Ω resistors. This arrangement provides adequate thermal compensation as hoop and longitudinal strain values are to be subtracted from each other as previously discussed.

3.3 Heating rate calibration series

A necessary step in the validation of the test setup was calibrating the system to have predictable interior heating rates as a function of the electrical power output of the heaters. Calibration tests were performed on the test chamber at electrical power values ranging from 468 W to 1,872 W by varying the input voltage to the electrical heaters with a variable autotransformer. Four tests were conducted by heating the chamber for 60 min at power settings corresponding to 20%, 40%, 60%, and 80% of maximum. All tests started with zero gauge pressure and the chamber at room temperature. Temperature and pressure data were recorded throughout. While setting the heaters at a constant power is inherently a transient process, temperature increases can be approximated as linear to provide a nominal heating rate useful in comparison to other calorimetry testing on lithium batteries. Interior gas temperature increases and associated linear fits for this calibration testing are shown in Figure 3.3(a). The nominal heating rates for the calibration tests follows a highly linear relationship with the heater setting as seen in Figure 3.3(b) which provides confidence in the ability to interpolate between power settings. Extrapolation of the data yields a maximum possible rate of 6.51 °C/min at the maximum heater setting of 2,340 W. However, tests will likely be kept below this rate to minimize the risk of heater failures.

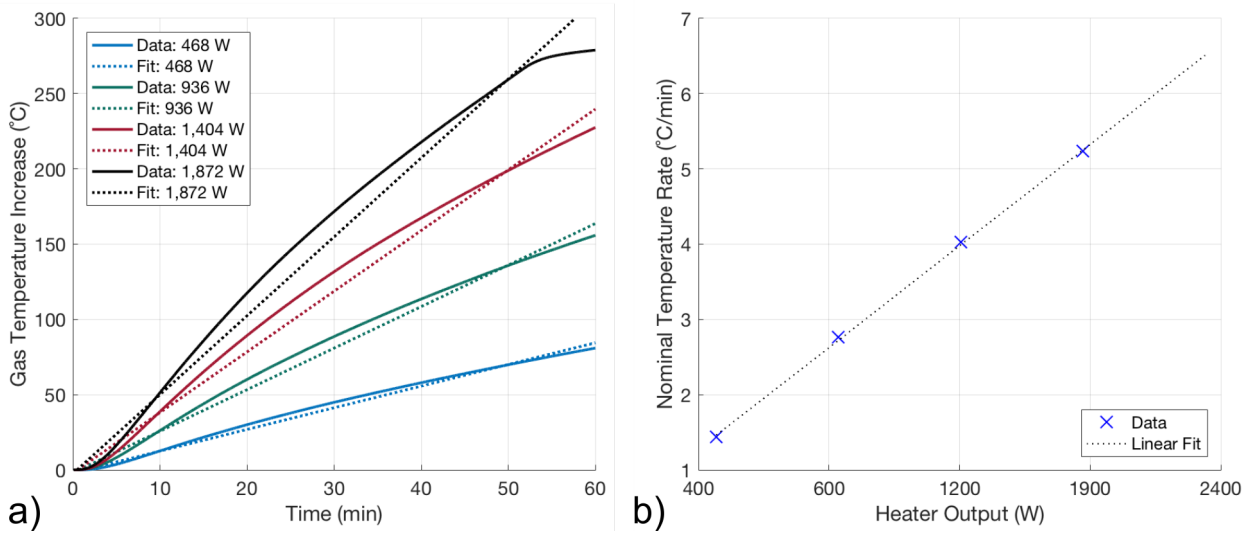

Figure 3.3: (a) Gas temperature increase versus time and linear fits for the heating rate calibration test series, and (b) plotting the nominal heating rate versus electrical power input for these tests.

3.4 Planned initial test series

An initial test series is planned with lithium cobalt oxide LG HE2 cells which should provide a strong baseline for comparison with other battery chemistries. This series will involve using cells charged to 100% SOC by performing charge and discharge cycles. Cells will be subjected to thermal abuse at a rate of 2 °C/min and 5 °C/min until failure is observed via the onset of venting. Trials will be performed at both heating rates with multiple pairs of strain gauges attached to individual cells to evaluate if there are any localized strain variations. Additional trials will be performed with a single pair of strain gauges on each battery and repeated in triplicate to determine the variation in strain and pressure trends during failure between cells of the same type.

4 Summary and conclusions

Understanding the internal pressure of a lithium battery under abuse conditions leading up to and at failure is an important metric in describing safety risks and how the external fluid dynamics of the venting process occurs. Two complementary experiments for describing the internal pressure of 18650 format lithium batteries have been developed and presented here. Both experiments are versatile in the use actual batteries or their components and are not limited to any certain brands or cell chemistries.

A test apparatus has been built to directly pressurize vent caps removed from live batteries to measure burst pressure and opening area. A series of validation tests has been performed which demonstrates the accuracy of the test setup with circular orifices and the more complicated vent geometries seen on actual batteries. The second experiment uses strain gauges to non-invasively infer the internal pressure within cells which can be subjected to various rates of thermal abuse. This test apparatus has been constructed and

calibrated.

References

[1] P.S. Grant, Spray Forming, Progress in Materials Science 39 (1995) 497-545.

[2] R.D. Reitz, F. V. Bracco, Mechanisms of Breakup of Round Liquid Jets. In *Encyclopedia of Fluid Mechanics*, Gulf Publishing Company, Houston, 1986.

[3] E. P. Roth, C. C. Crafts, D. H. Doughty, J. McBreen, Sandia Report SAND2004-0584 (2004).

[4] D. P. Finegan, M. Scheel, J. B. Robinson, B. Tjaden, I. Hunt, T. J. Mason, J. Millichamp, M. DiMichiel, G. J. Offer, G. Hinds, D. J. L. Brett, P. R. Shearing, In-operando high-speed tomography of lithium-ion batteries during thermal runaway, Nature Communications 6:6924 (2015) 1-10. doi:10.1038/ncomms7924

[5] P. T. Coman, S. Rayman, R. E. White, A lumped model of venting during thermal runaway in a cylindrical Lithium Cobalt Oxide lithium-ion cell, Journal of Power Sources 307 (2016) 56-62. doi:10.1016/j.jpowsour.2015.12.088

[6] J. D. Anderson, Modern Compressible Flow with Historical Perspective, Third Edition, McGraw Hill, Boston, 2003.

[7] P. Hill, C. Peterson, Mechanics and Thermodynamics of Propulsion, Second Edition, Pearson, 1991.

[8] W. C. Young, R, G, Budynas, Roark's Formulas for Stress and Strain, Seventh Edition, McGraw Hill, New York, 2002.

[9] A. P. Boresi, R. J. Schmidt, Advanced Mechanics of Materials, Sixth Edition, Wiley, Hoboken, 2003.

[10] F. P. Beer, E. R. Johnston Jr., J. T. DeWolf, D. F. Mazurek, Mechanics of Materials, Fifth Edition, McGraw Hill, New York, 2006.